J Mater Sci (2018) 53:10442–10456

Metals

Superior strength and ductility of 316L stainless steel with heterogeneous lamella structure

Jiansheng Li[1], Yang Cao[1], Bo Gao[1], Yusheng Li[1,*], and Yuntian Zhu[1,2]

[1] *Nano and Heterogeneous Materials Center, School of Materials Science and Engineering, Nanjing University of Science and Technology, Nanjing 210094, China*
[2] *Department of Materials Science and Engineering, North Carolina State University, Raleigh, NC 27695, USA*

Received: 8 February 2018
Accepted: 11 April 2018
Published online: 17 April 2018

ABSTRACT

Strength and ductility are two of the most important mechanical properties for a metal, but often trade off with each other. Here, we report a 316L stainless steel with superior combinations of strength and ductility that can be controlled by fine-tuning its heterogeneous lamella structure (HLS). The HLS was produced by 85% cold rolling, which produced lamellar coarse grains sandwiched between mixtures of nano-grains and nano-twins. The HLS was fine-tuned by annealing at 750 °C for 5–25 min, which resulted in varying volume fractions of nano-grains, nano-twins, lamellar coarse grains, and recrystallized grains. During tensile testing, large amount of geometrically necessary dislocations were generated near the heterostructure interfaces to coordinate the deformation between soft domains and hard domains, which results in high back stress to achieve superior combination of strength and ductility. An optimal high yield strength of ~ 1 GPa with an elongation-to-failure of ~ 20% was obtained for an optimized HLS sample. Furthermore, the processing technique employed here is conducive to large-scale industrial production at low cost.

Introduction

316L stainless steel is a widely used engineering material because of its combination of excellent corrosion resistance, great oxidation resistance, and good formability [1]. However, the relatively low strength (yield strength of 200–400 MPa in annealed states) limits it from engineering application with a higher requirement [2]. In recent decades, many technologies such as cold rolling (CR) [3, 4], surface mechanical attribution (SMAT) [5, 6], equal channel angular pressing (ECAP) [7–11], and high-pressure torsion (HPT) [12, 13] have been explored to obtain ultrafine-grained/nanocrystalline bulk metals to significantly improve the strength of stainless steels and other alloys. Unfortunately, strength enhancement by grain refinement is inevitably accompanied with a sacrifice in ductility, which increases the potential for catastrophic failure during service.

Approaches to process the stainless steel for high strength and good ductility are urgently needed. In fact, the mechanical properties of metallic materials

Address correspondence to E-mail: liyusheng@njust.edu.cn

https://doi.org/10.1007/s10853-018-2322-4

are determined by their internal microstructures and external environmental conditions. Many efforts have been reported to optimize microstructure to achieve a good combination of strength and ductility [14–17]. Fang et al. [18] reported that the tensile behavior of Cu can be effectively enhanced by introducing the gradient structures (spatial variation of grain sizes). The gradient nano-grained Cu exhibited one time higher yield strength and a tensile elongation-to-failure of ~ 60%. Similar superior strength–ductility combinations were also found by Wu et al. [19, 20] for the gradient structured IF and 304 stainless steel. The high ductility was attributed to extra strain hardening due to the presence of strain gradient and the change of stress states, which generated geometrically necessary dislocations (GNDs) and promoted the multiplication and interaction of forest dislocations [14, 21].

Another strategy to successfully obtain high strength and good ductility was reported by Wang et al. [22] who developed a thermomechanical processing route to obtain bimodal grains of Cu with micrometer-sized grains randomly embedded among ultrafine grains. They attributed the excellent mechanical property for the action of hard ultrafine grains and numerous GNDs from the ultrafine coarse grain boundaries (soft/hard interfaces). The similar enhanced mechanical property was also obtained for bimodal Fe–Cr–Ni alloys [23]. Ameyama and co-workers [24] further redesigned the bimodal grains to harmonic structure with continuous three-dimensional network of hard ultrafine-grained skeleton filled with islands of soft coarse-grained regions. The high ductility was associated with ultrafine-grained network (soft/hard interfaces). These reports show the advantage of introducing heterostructures in producing good strength and ductility in metals [25].

More recently, heterogeneous lamella structures (HLSs) prepared by simple cold rolling and annealing were reported to markedly enhance the strength and ductility of Ti and 301 stainless steel [26, 27]. Unusual high strength was obtained with the assistance of high back stress, whereas high ductility was attributed to back-stress hardening and dislocation hardening [26]. For the 316L austenite stainless steel, a combination of 1.0 GPa tensile strength and an elongation-to-failure of ~ 27% was achieved in the annealed dynamic plastic deformation (DPD) sample [28]. However, this technique is associated with high cost and limited sample size, which makes it challenging to process materials large enough for real industrial applications. Hirota et al. [29] found the HLS in 316L stainless steel during the process of exploring the recrystallization and grain growth behavior, but the mechanical behaviors were not reported. Belyakov et al. [30] indicated that the 316L stainless steel with HLS possessed enhanced strength and ductility, but its mechanism was not studied. HLS is considered one of the most effective structures that produce high strength and high ductility [31].

In the present work, 316L stainless steel samples with heterogeneous lamella structures were prepared by means of conventional cold rolling for a strain of 85% and subsequent annealing. Their structural evolution and mechanical properties are reported herein.

Experimental

Characterization of the as-received sample

The material used in this study was a hot rolled 316L stainless steel sheet with a thickness of 10 mm. Its chemical composition is listed in Table 1. Figure 1 shows equiaxed austenitic grains and significant amount of annealing twins in its as-received state. The grain size distribution is presented in Fig. 1b, and the average grain size is around 35 μm.

Preparation of HLS

The as-received 316L stainless steel sheets were processed by conventional cold rolling at room temperature on a rolling mill with 400-mm-diameter rolls. Both rolls were driven at the same velocity of ~ 335 mm/s, and the mean thickness reduction was ~ 0.17 mm per pass. The sample sheets were rolled from 10 to 1.5 mm thick after 50 passes with a total rolling reduction of ~ 85% and then annealed at 750 °C under nitrogen protection for 5, 10, 15, 20, and 25 min for partial recrystallization.

Microstructure analysis

An automated Bruker-AXS D8 Advance diffractometer with Cu Ka radiation was used to obtain X-ray diffraction (XRD) patterns to study possible phase transformation. 2-Theta ranges from 40° to 100°, and the scanning speed was 6°/min. A field emission scanning electron microscope (SEM, Quant

Table 1 Chemical compositions of 316L stainless steel

Material	Chemical compositions (wt%)												
	Cr	Ni	Mo	C	Si	Mn	S	P	Co	Cu	Nb	W	Fe
316L	16.47	10.10	1.97	0.030	0.530	1.42	0.005	0.030	0.244	0.146	0.012	0.031	Bal.

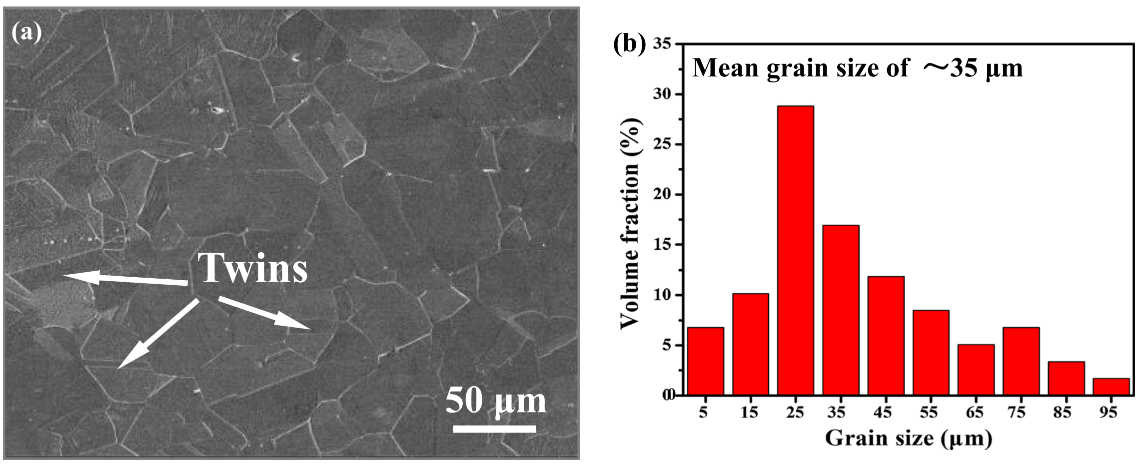

Figure 1 Microstructure of the as-received 316L stainless steel: **a** SEM micrograph, indicating the existence of many annealing twins and **b** the volume fraction distribution of the original coarse grains. It is noted that twin boundaries are not counted when making the grain size distribution.

250 FEG) was used to characterize the fractured surface. Electron back-scattered diffraction (EBSD) was carried out in a Zeiss Auriga scanning electron microscope (SEM). The step size was 50 nm, and scanning voltage was 15 kV. HLSs were characterized on a TECNAI G2 20 LaB6 transmission electron microscope (TEM) at an accelerated voltage of 200 kV. The as-received TEM specimens with a thickness of 0.5 mm were cut from the sample cross section by wire electrode cutting and then mechanically grinded down to a thickness of $\sim$ 50 μm. The final thinning was accomplished by a twin-jet electrochemical polishing in a solution of 8% perchloric acid + 92% ethanol at 50 V (80 mA) and around − 10 °C. The measurements of average grain size and volume fraction of the micro/nano-grains were completed with a Nano Measurer and Photoshop software, respectively.

Mechanical property tests

Vickers hardness was measured by a HMV-G hardness tester with a load of 200 g and a holding time of 15 s. Hardness values were obtained by averaging at least ten indents for each sample. The treated 316L sheets were cut along the rolling direction into dog-bone-shaped specimens, with gage length of 20 mm, width of 3 mm, and final polished thickness of 1.5 mm. Uniaxial tensile tests were performed on an electromechanical universal testing machine (LFM-20kN) with a strain rate of 3×10^{-3} s^{-1} at room temperature. All tests were performed three times under the same condition to guarantee the data consistency.

Results

Microstructures

XRD analysis

XRD data are shown in Fig. 2a. The as-received sample is composed of austenite phase (γ, 95.6% in volume) and martensite phase (α′, 4.6% in volume). After 85% cold rolling, the volume fraction of martensite phase was increased to 26.4%, due to the strain-induced martensite transformation [32–34]. Usually, the martensite phase is not stable in 316L

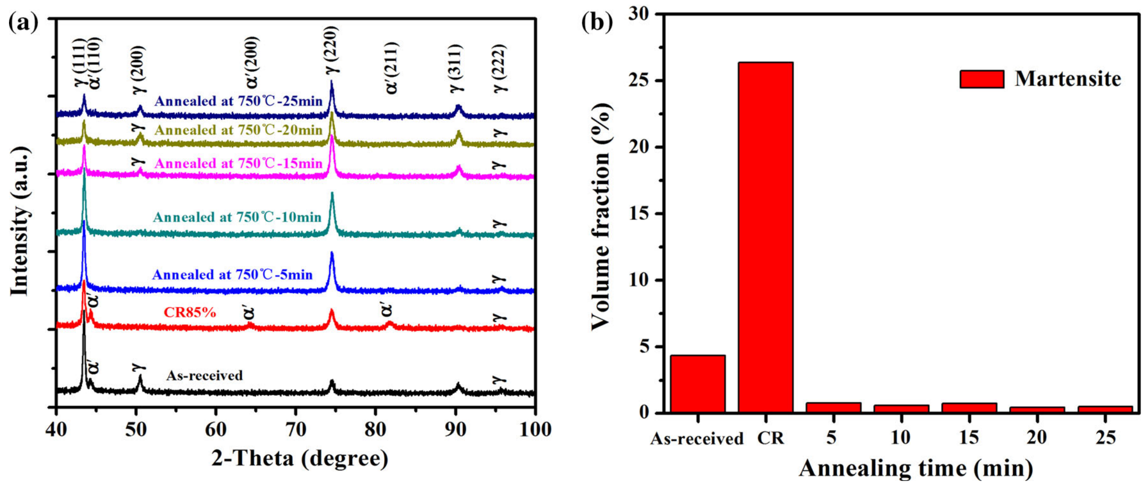

Figure 2 **a** XRD data of the as-received and treated 316L stainless steels (γ is austenite phase and α' is martensite phase) and **b** the volume fraction of martensite as a function of annealing time.

stainless steel, especially at high temperature (> 700 °C). Roland et al. [35] reported that the volume fraction of martensite reached a minimum value of 5% after annealing at 700 °C. In this study, annealing at 750 °C effectively eliminated the martensite phase (below 1%) to produce single austenite phase. The volume fractions of martensites are exhibited in Fig. 2b, and the detailed calculation can be found in previous work [36].

Microstructural evolution characterized by EBSD

Figure 1a shows the microstructure of the as-received sample with largely equiaxed austenitic grains and a significant amount of annealing twins. After 85% cold rolling, the original coarse-grained (CG) structure was morphed into HLS, which is composed of the ultrafine grains (UFGs, hard to be identified by EBSD in Fig. 3a) and lamellar coarse grains (LCG). As shown in Fig. 3a1 for its enlarged image (from the yellow-framed area in Fig. 3a), the lamellar coarse grains are sandwiched between UFG domains that mainly consist of elongated subgrains and shear bands (SBs, ~ 45° to rolling direction). Previous studies [37, 38] have confirmed that the refined grains were formed by shearing of the lamellar coarse grains, which will be discussed in "Formation and evolution mechanisms of HLS" section. After it was annealed at 750 °C for 5 min, nearly no obvious change of EBSD morphology was found, compared to that of the deformed sample (Fig. 3b). However, when the annealing time was increased to 10 min, a remarkable change in microstructure took place. Figure 3c shows some equiaxed recrystallized grains (RGs) in the UFG region and they inclined to form lamellar clusters, while the original lamellar coarse grains changed very little. When the annealing time increased to 15 min, the UFG domains mostly transformed into recrystallized grains, forming HLS with soft recrystallized domains and original lamellar coarse-grained domains, as shown in Fig. 3d. For the sample annealed for 25 min, the recrystallized grain lamellae grew further and lamellar coarse-grained domains nearly vanished, which can be clearly seen in Fig. 3e.

Figure 4a is the TEM image of lamellar coarse grain in the deformed sample. Numerous dislocation walls induced by shear stress are presented, which resulted in a distorted selected area diffraction pattern (the inset a2 in Fig. 4a). It should be emphasized that a distinct shear band with 45° to rolling direction traverses the whole lamellar coarse grain. Some previous works [37, 38] attributed the refinement of coarse grains during severe deformation process to the drastic shear effect in the shear bands. The selected area diffraction pattern (the inset a1 in Fig. 4a) further confirms that the ultrafine grains are produced within the shear bands. Figure 4b shows typical morphologies of the UFG areas, which can be characterized as some nano-twin bundles embedded in the nano-grained matrix. The distributions of their transverse grain sizes are presented in Fig. 4c and d, respectively. It reveals that the average transverse

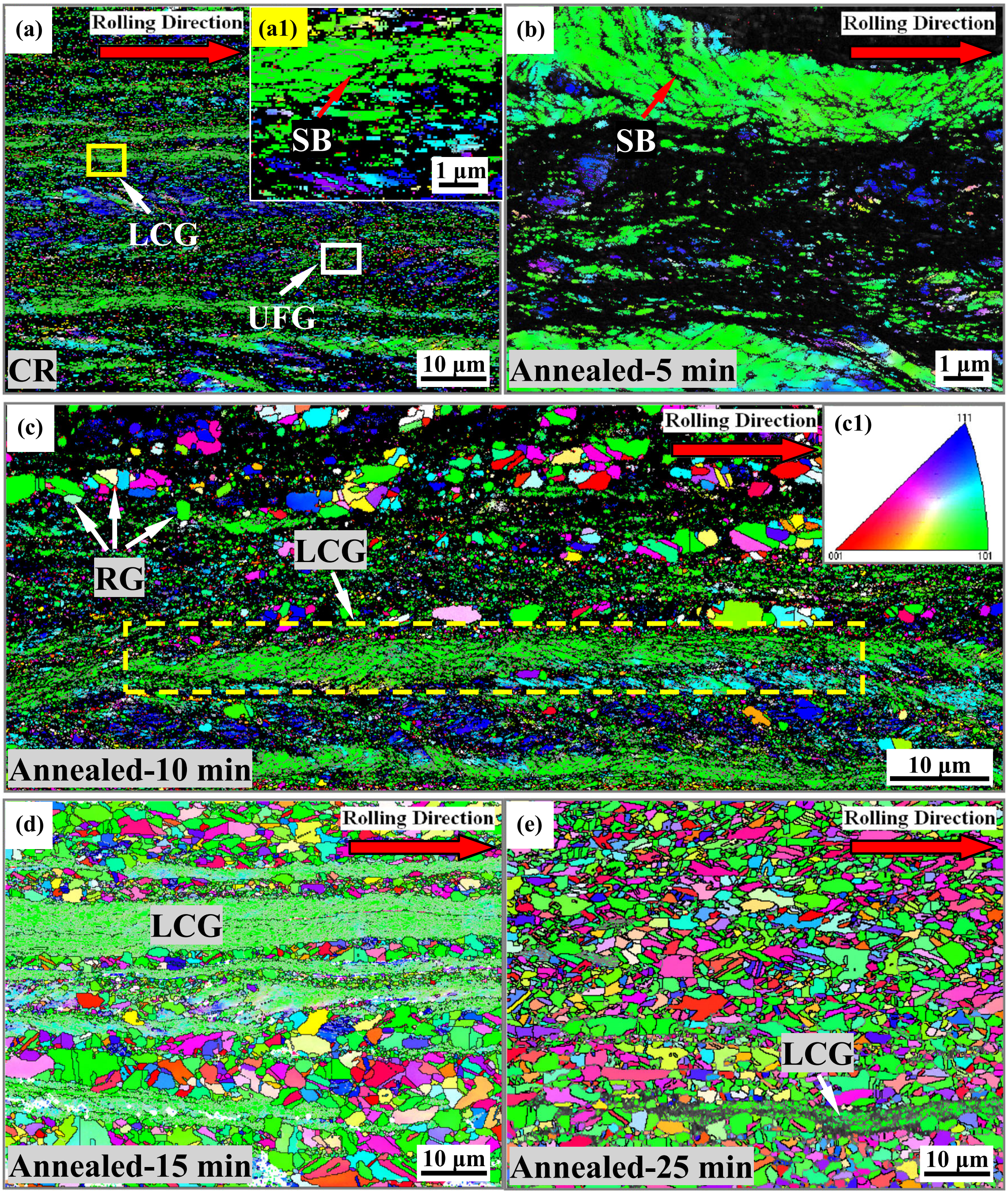

Figure 3 EBSD orientation maps of treated 316L stainless steels: **a** 85% cold rolling (CR), **b** CR + annealing at 750 °C for 5 min, **c** CR + annealing at 750 °C for 10 min, where the inset is inverse pole figure, **d** CR + annealing at 750 °C for 15 min, and **e** CR + annealing at 750 °C for 25 min.

size of nano-grains is ~ 46 nm and the twin/matrix lamellar thickness is ~ 22 nm.

Annealing at 150 °C for 10 min led to the nucleation and growth of recrystallized grains forming lamellar domains (Fig. 5a), which is consistent with the result in Fig. 3c. The recrystallized grains have sizes in the range of 0.4–3.6 μm (averagely 0.69 μm) and are equiaxed and dislocation free. Figure 5b shows that an unrecrystallized region consists of the nano-twins and nano-grains. It is noted that the recrystallization first occurred in regions with high stored energies, such as the regions with nano-grains

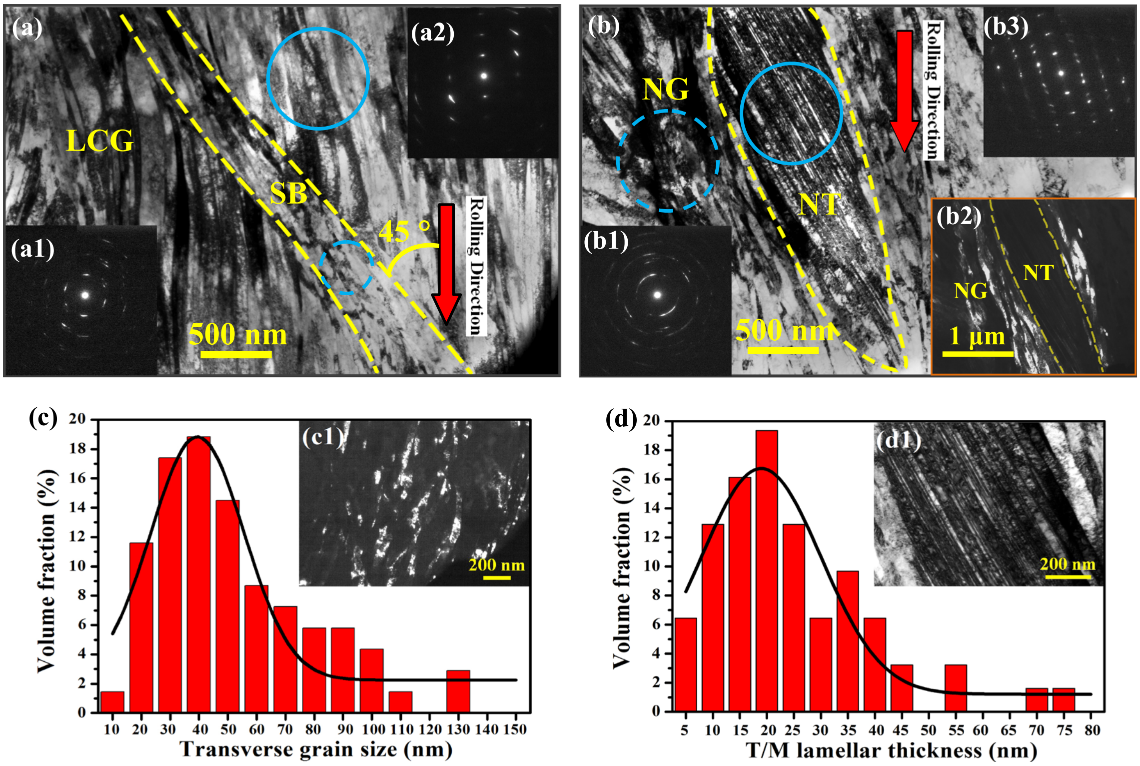

Figure 4 Typical cross-sectional TEM image of 85% rolled 316L stainless steel: **a** the TEM image of the lamellar coarse grain (LCG), the inset **a1** is selected area diffraction pattern of shear band (SB, circled by blue dashed line), the inset **a2** is selected area diffraction pattern of lamellar coarse grain (circled by blue line), **b** the TEM image of nano-twin (NT) bundle surrounded by nano-grains (NGs), the inset **b1** is the selected area diffraction pattern of NGs (circled by blue dashed line), the inset **b2** is the dark-field image of **b**, the inset **b3** is selected area diffraction pattern of NT bundle (circled by blue line), and **c** and **d** are the distributions of transverse grain sizes of NG and NT, respectively.

and nano-twins. Donadille and Schino et al. [39, 40] reported that severely deformed regions have high driving force to accelerate the nucleation and growth of recrystallization. As shown in Fig. 5c and d, the mean size of nano-twins after annealing increased from ∼ 22 nm (as-CR) to ∼ 50 nm and mean size of nano-grains from ∼ 46 nm (as-CR) to ∼ 89 nm.

After annealing at 750 °C for 25 min, the microstructure consists of mostly equiaxed recrystallized grains (Fig. 6a), in the size range of 1–8 μm, average size of 1.96 μm, and volume fraction of > 90%. The annealing also produced large quantity of submicro-twins with thickness in the range of 100–800 nm. Figure 6b shows small amount of residual lamellar coarse-grained domains, which demonstrates the excellent thermal stability of the lamellar coarse-grained structure [41]. Figure 6c and d further elucidates that these residual lamellar coarse grains contain numerous dislocation cells, which might be from the rearrangement of the dislocation walls (Fig. 4a) during annealing treatment.

Mechanical properties

Microhardness

Figure 7 gives the variation in microhardness of 316L stainless steel with different treatment histories. As shown in the upper right inset, the as-received 316L sample has a low hardness of 177 Hv. After 85% cold rolling, it achieved extremely high hardness of 441 Hv, which exceeds the level of the nanostructured DPD 316L stainless steel [28]. During the annealing at 750 °C, the hardness decreased with duration in a typical "S" shape, following the classical Johnson–Mehl–Avrami relation [42]. The microhardness values after 5, 10, 15, and 20 min annealing are 408, 373, 292, and 263 Hv, respectively, and eventually tend to a saturation value of ∼ 250 Hv.

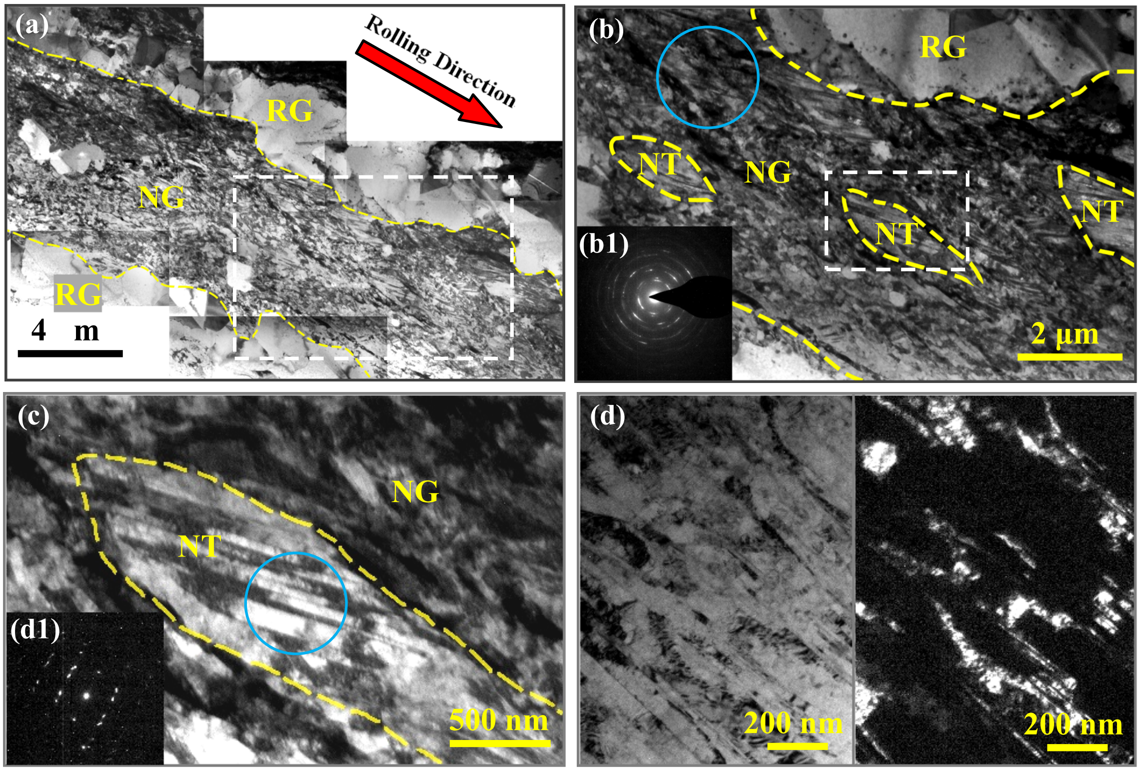

Figure 5 **a** typical cross-sectional TEM image of 316L stainless steel annealed at 750 °C for 10 min, **b** the enlarged TEM image of the selected region (the white dashed rectangle) in **a**, the inset is the selected area diffraction pattern (circled by blue line) of nano-grains (NGs), **c** the enlarged TEM image of the selected region (the white dashed rectangle) in **b**, the inset is the selected area diffraction pattern (circled by blue line) of nano-twins (NTs), and **d** the bright-field and dark-field images of NGs.

Tensile behaviors

Typical engineering stress–strain curves of treated 316L samples are present in Fig. 8a, and the detailed tensile properties are summarized in Table 2. The yield strength of cold-rolled sample is 1421 MPa, which is three times higher than that of the as-received sample. However, its low ductility is a roadblock to its practical applications. Figure 8b shows that the sample failed in a typical brittle manner without dimples while the typical ductile fracture is found for as-received sample (dimples taken from central fractograph with the mean sizes of ∼ 5 µm). Meanwhile, an obvious decrease in tensile yield/ultimate strength and an increase in ductility are observed after annealing (Fig. 8a and Table 2). Annealing for 5 min induced a distinct drop in yield strength (from 1421 to 1108 MPa), accompanied with an increment in elongation-to-failure of ∼ 4%, but without an obvious improvement in uniform elongation (∼ 0.5%). Typical brittle fractography is also observed for the 5-minute-annealed sample (Fig. 8b). For the sample annealed for 10 min, the yield strength dropped to ∼ 1 GPa, and the elongation-to-failure increased dramatically to ∼ 20% with an uniform elongation of ∼ 9%. This indicates that the deformed 316L stainless steel annealed at 750 °C for 10 min possesses superior combination of strength and ductility. A large number of tiny dimples with the mean sizes of ∼ 1 µm exist on the fracture surface, which is consistent with the good ductility of the 10-minute-annealed sample. As the annealing duration is increased to 15, 20, and 25 min, ductility increased further by strength dropped dramatically (below 670 MPa).

Discussion

Formation and evolution mechanisms of HLS

Based on the experimental observations, we propose and illustrate the formation and evolution processes of the HLS in treated 316L stainless steel in Fig. 9. The

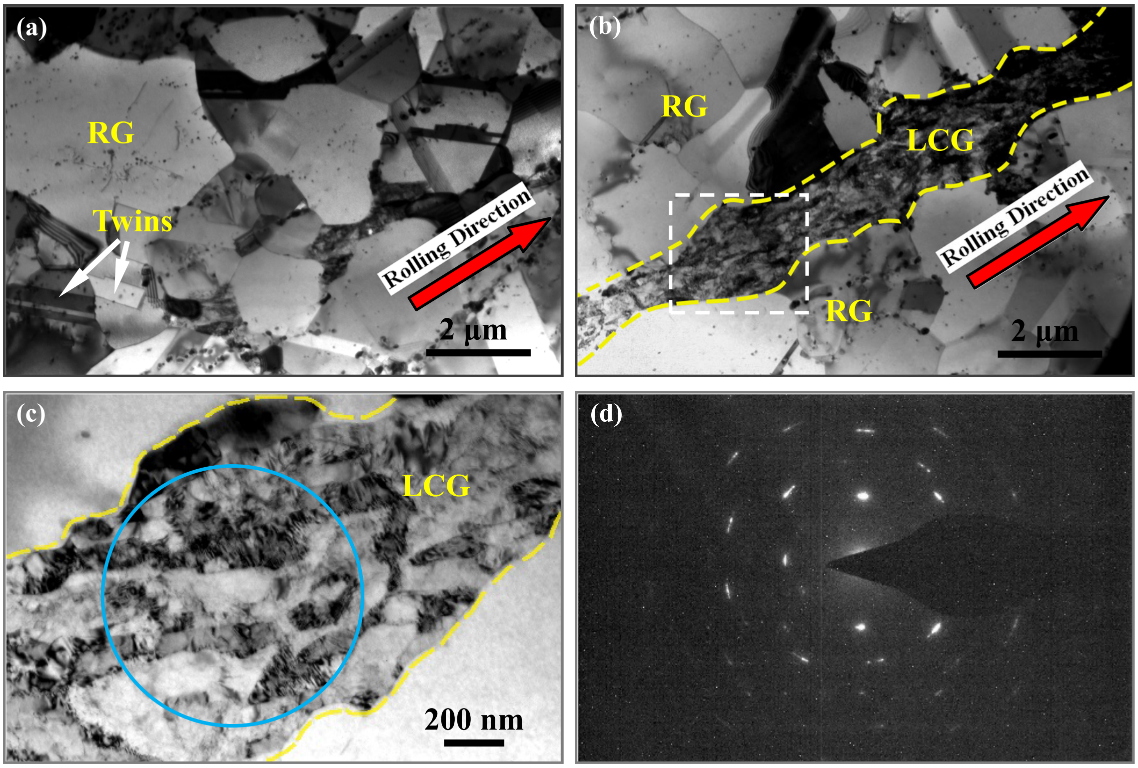

Figure 6 **a** typical cross-sectional TEM image of 316L stainless steel annealed at 750 °C for 25 min, **b** TEM image with residual lamellar coarse grain (LCG), **c** the enlarged TEM image of the selected region (the white dashed rectangle) in **b**, and **d** the selected area diffraction pattern (circled by blue line) of lamellar coarse grain in **c**.

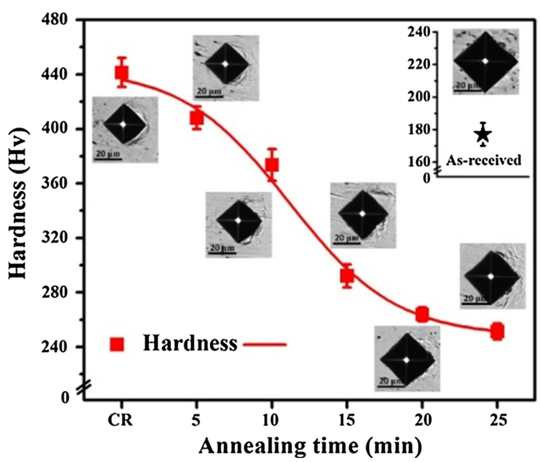

Figure 7 Variations in hardness of the 316L stainless steels with annealing time at 750 °C, and the inset is the hardness of the as-received 316L sample.

original HLS formed after 85% cold rolling consists of the lamellar coarse grains sandwiched between nano-grain/nano-twin domains (Fig. 9b). During the cold rolling, equiaxed coarse grains become elongated in the flow direction [43, 44]. Meanwhile, many primary micro-twins and subgrains were rapidly formed at early stage of deformation [45, 46], and they will be further refined to form ultrafine twins and grains at higher strain [47]. Further deformation led to the formation of shear bands, which separated the matrix with a pair of sharp boundaries across the lamellar coarse grains at 45° to the rolling direction (Fig. 3a and Fig. 4a) [48]. Figure 10 further confirms the formation of nano-grains by cutting twin bundles and deformed austenitic matrix in shear bands, which produced nano-martensite/ austenite grains. Meyers and Xue et al. [37, 49] also reported that nano-twins, elongated ultra-laths, and equiaxed ultrafine grains can be commonly created in shear bands due to the formation of secondary nano-twins and shear fracture of the primary micro-twins or the elongated subgrains, which form the observed nano-twin/-nano-grain lamellar structure. In fact, deformation is always initiated in some grains with lower Schmid factor. The existence of residual lamellar coarse grains may be related to the initial orientation of these coarse grains.

Ultrafine/nano-grains in metallic materials are believed metastable. The recrystallization nucleation

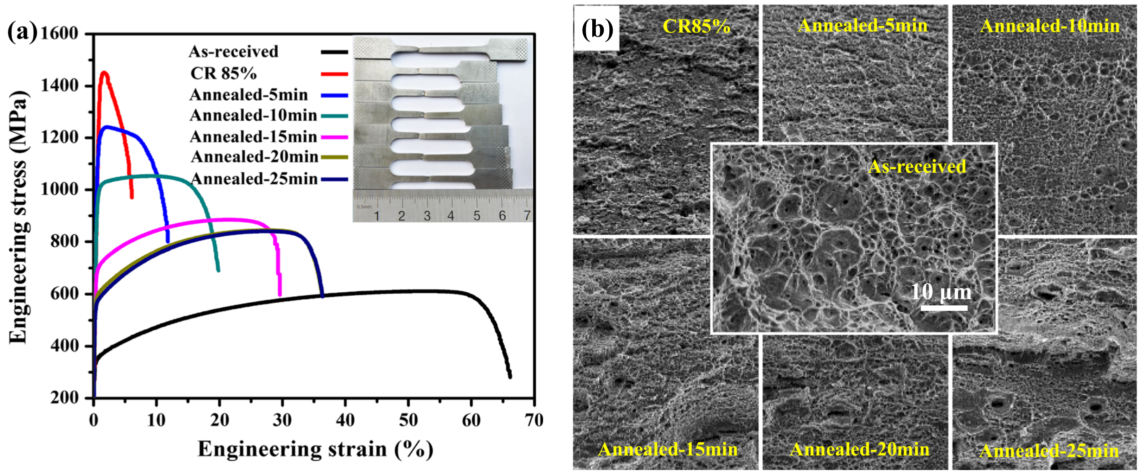

Figure 8 **a** tensile engineering stress–strain curves of as-received and treated 316L stainless steels and **b** the central fractographs of the as-received and treated 316L stainless steels.

Table 2 Tensile properties of the as-received and treated 316L stainless steels

316L	UTS (MPa)	YS (MPa)	FE (%)	UE (%)
As-received	621 ± 10	356 ± 16	63.1 ± 2.6	53.4 ± 2.0
CR 85%	1451 ± 6	1421 ± 13	5.9 ± 0.7	1.6 ± 0.1
Annealed for 5 min	1242 ± 5	1108 ± 112	10.0 ± 1.4	2.1 ± 0.1
Annealed for 10 min	1059 ± 5	1000 ± 10	19.4 ± 1.5	9.0 ± 0.5
Annealed for 15 min	882 ± 11	662 ± 16	29.2 ± 0.7	21.2 ± 0.3
Annealed for 20 min	842 ± 4	603 ± 35	36.3 ± 0.5	26.5 ± 1.5
Annealed for 25 min	849 ± 8	572 ± 16	36.1 ± 1.7	27.5 ± 1.3

usually prefers to occur in regions with high stored energy. For annealing at 750 °C, since the nano-twins have higher thermal stability (lower stored energy) in comparison with nano-grains [28], recrystallization may occur preferentially in nano-grained regions instead of nano-twin bundles. This hypothesis is confirmed by the observation that the nano-twin bundles largely survived while nano-grains mostly vanished (Fig. 11).

As shown in Figs. 3c and 5a, recrystallized grains were inclined to form in deformed matrix with lamellar cluster structure, which is consistent with the result of Hirota et al. [29]. Yan et al. [28] also reported that shear bands with high stored energy tend to form lamellar domain consisting of recrystallized grain clusters. In the unrecrystallized regions, there are slight nano-grain growth and nano-twin thickening with increasing annealing time (Figs. 4, 5). This suggests that some extremely fine nano-grains coalesced through grain boundary migration [50]. Longer annealing duration led to the disappearance of both nano-grains and nano-twin bundles (Figs. 6, 9d). Therefore, subsequent recrystallization may occur in narrow shear bands in the lamellar coarse grains, which gradually devours them. The final HLS is composed of micrometer recrystallized grains and the residual lamellar coarse grains (Fig. 6b). The volume fractions of various microstructures in the treated 316L stainless steels are illustrated in Fig. 11. It also indirectly displays the evolution process of the HLS.

Enhanced strength and ductility

The conventional cold rolling with subsequent short annealing can effectively control the formation and evolution of HLS in 316L stainless steel, which produced superior combinations of strength and ductility (Fig. 12a) over those reported in previous works for samples processed by CR, hot rolling (HR), SMAT, annealed HR/CR, and comparable to those processed by DPD and annealing [6, 28, 33, 35, 36, 51, 52]. However, DPD can only produce small samples. The current technique has great potential for industrial application with low cost.

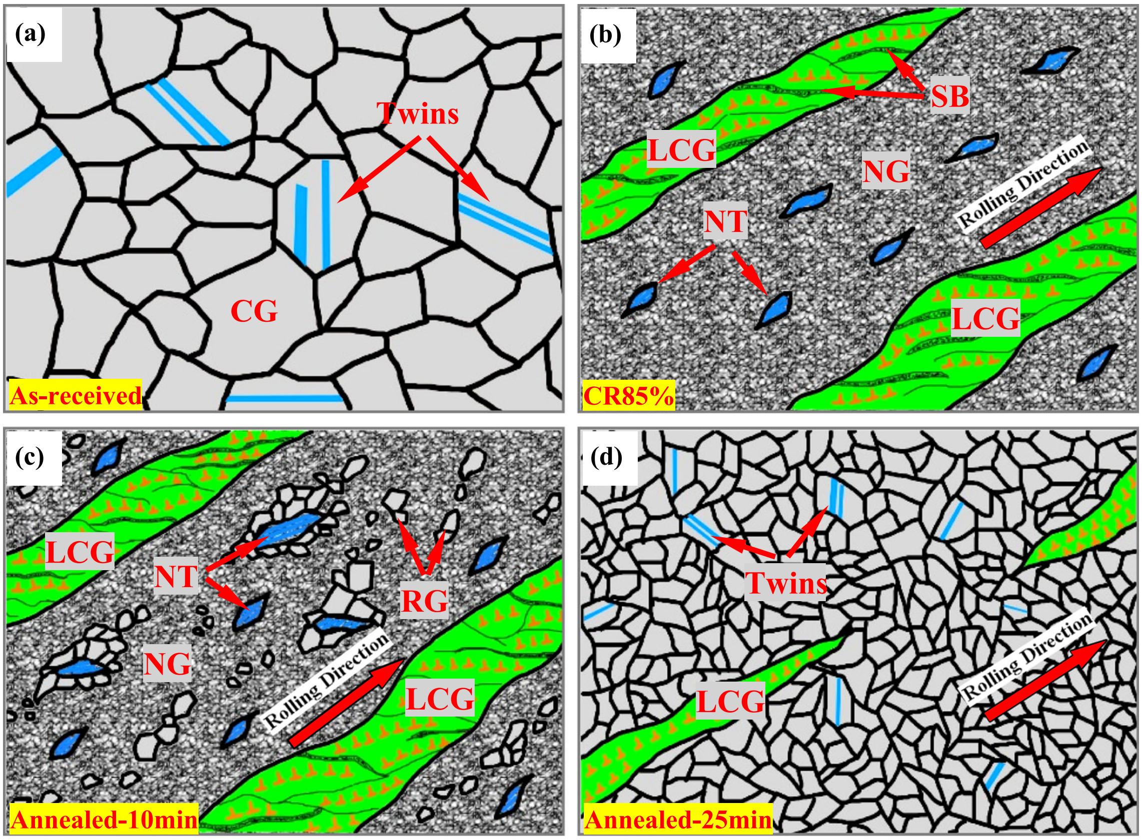

Figure 9 A schematic representation of the formation mechanism of HLS.

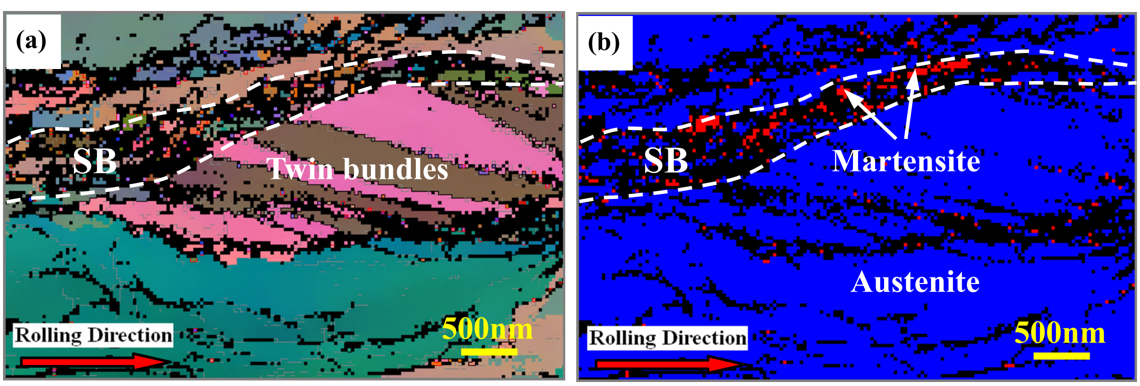

Figure 10 **a** EBSD image of the lamellar coarse grain in deformed 316L stainless steel and **b** the corresponding phase distribution of **a**, where the red phase is martensite and the blue phase is austenite.

The strength of metallic materials is traditionally estimated using the rule of mixture, i.e., the sum of the strength of each structural components weighed by their volume fraction [53]. However, for the HLS structure, the synergistic strengthening caused by the interaction between the soft and hard heterogeneous domains, $\Delta\sigma^{\mathrm{Syn}}$, should be included [26, 53], which leads to the following equation:

$$\sigma_{\mathrm{Y}} = f^{\mathrm{LCG}}\sigma_{\mathrm{Y}}^{\mathrm{LCG}} + f^{\mathrm{RG}}\sigma_{\mathrm{Y}}^{\mathrm{RG}} + f^{\mathrm{NT}}\sigma_{\mathrm{Y}}^{\mathrm{NT}} + f^{\mathrm{NG}}\sigma_{\mathrm{Y}}^{\mathrm{NG}} + \Delta\sigma^{\mathrm{Syn}}, \quad (1)$$

where f represents volume fraction, σ_{Y} the yield strength, LCG the lamellar coarse grains, RG the recrystallized grain, NT the nano-twin, and NG the nano-grain. It should be noted that Eq. (1) can only be used to estimate the strength. Since domains that yield at higher strength will mean yielding at higher

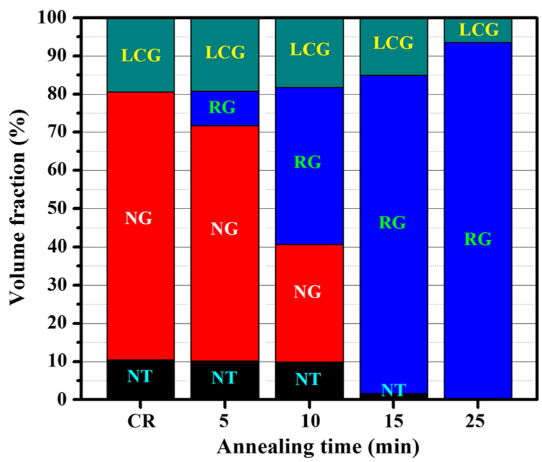

Figure 11 Volume fractions of various microstructures in treated 316L stainless steels.

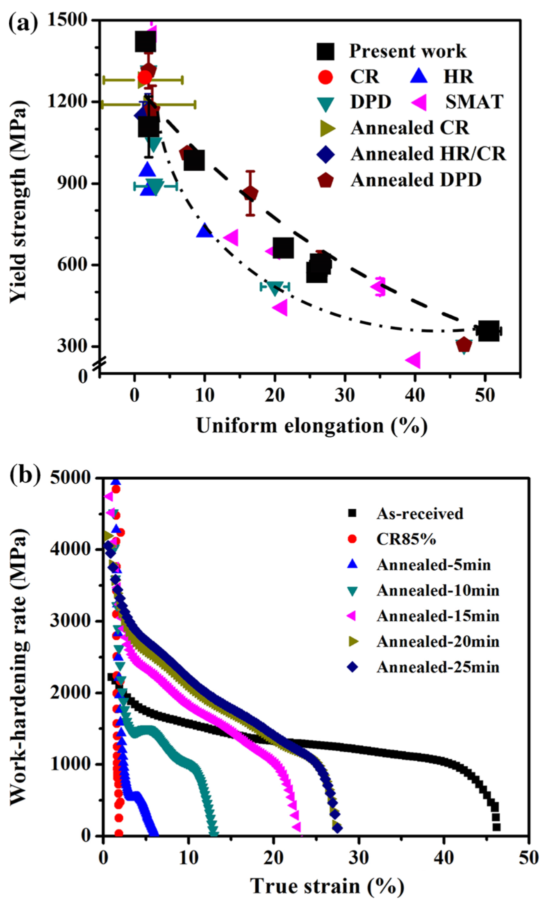

Figure 12 **a** correlations between yield strength and uniform elongation for the 316L stainless steels in the present and other works: HR [51], CR [52], DPD [28], SMAT [6, 35, 36], annealed CR [52], annealed HR/CR [33], annealed DPD [28], **b** work-hardening rates of the as-received and treated 316L stainless steels in the present works.

strain, it is logically problematic to simply add the weighted strength of different domains together. For heterostructured materials, the $\Delta\sigma^{Syn}$ contribution could be significant [26, 53].

Twin boundary is a coherent and stable interface that can strongly obstruct slip transfer of dislocations, which greatly improves the yield strength [17, 54–56]. It is noted that the nano-twin bundles with average T/M lamellar thickness of ~ 30 nm possess higher yield strength (> 2 GPa [28]) than that (~ 1.45 GPa [6]) of nano-grains with a mean size of ~ 40 nm. As the 316L stainless steel annealed for 10 min, the recrystallized grains nucleated and grew at the cost of nano-grains, which lowers the strength. However, nano-twins were more thermally stable and kept nearly constant volume fraction (Fig. 11). This should have made much contribution to the high yield strength.

To estimate the strength using Eq. (1), the yield strength of lamellar coarse grain in Table 3 [6, 28, 57] is calculated with the value of 1003 MPa from CR85% 316L stainless sample. Then, the yield strength of lamellar coarse grain is assumed as a constant value for 10-minute-annealed 316L sample, which is an overestimation. The yield strength of 10-minute-annealed 316L stainless sample estimated using the first four terms is 945 MPa, which is still lower than the observed 1 GPa, despite the overestimation of the strength of lamellar coarse grains and nano-twins. This indicates that the $\Delta\sigma^{Syn}$ contribution is indeed significant here.

The excellent ductility for the treated 316L stainless steels is largely determined by the work-hardening capability [19, 26, 31, 58]. Work hardening can come from two different contributors: (1) The accumulation of crystalline defects such as dislocations, twins, and stacking faults, which makes further deformation harder. This is the primary contributor for conventional homogeneous materials. (2) Back stress increases with plastic straining. This contributor may become a primary contributor for heterostructured materials [31], such as the heterogeneous stainless steel in this study. Figure 12b shows the strain hardening with strain for samples annealed for different time periods. As shown, increasing annealing time generally improves the work-hardening ability, because (1) the recrystallized grains have more room to accumulate dislocations, and (2) back-stress hardening may increase when heterostructure is formed.

Table 3 Volume fractions and yield strengths of LCG, RG, NT, and NG in CR 85% and 10-minute-annealed 316L stainless steels

316L	LCG	RG	NT	NG	Total
Volume fraction of CR 85% (%)	19.4	0	10.5	70.1	100
Yield strength of CR 85% (MPa)	1003	–	2000 [28]	1450 [6]	1421 (Tested)
Volume fraction of annealed 10 min (%)	18.2	41.1	9.9	30.8	100
Yield strength of annealed 10 min (MPa)	1003*	~ 520	2000* [28]	~1140 [6, 57]	1000 (Tested)

*The data may be higher than the practical value for not taking consideration of the annealing effect

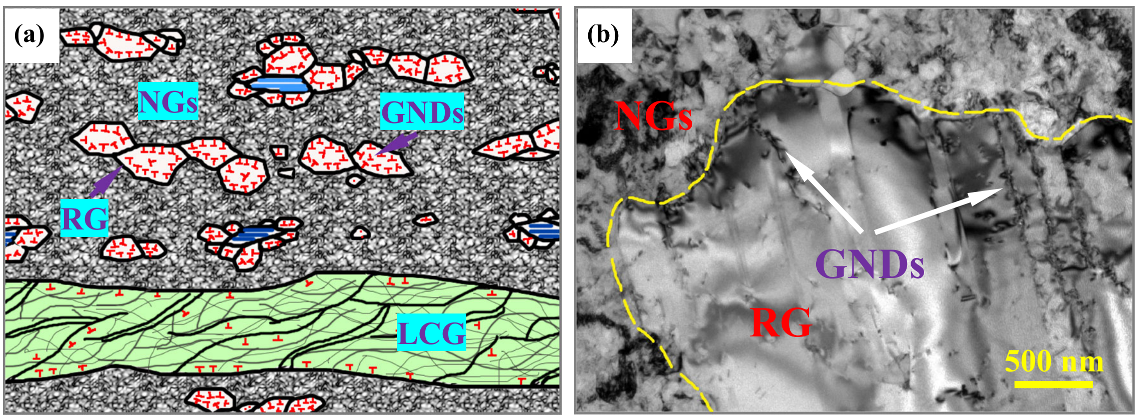

Figure 13 **a** schematic representation of generation of GND induced by various soft/hard interfaces and **b** TEM observation of GNDs in recrystallized grains with an engineering strain of 6.5% in 316L stainless steel annealed at 750 °C for 10 min.

As mentioned above, back-stress strengthening and back-stress work hardening should have played an important role in the observed superior mechanical properties. Two kinds of soft/hard domain interfaces exist in the HLSs (Fig. 13a). First, the soft recrystallized domains are surrounded by hard nano-grains/nano-twins. During the deformation, there will be strain gradient near their interfaces because of the big difference in their flow stress. The strain gradient will be accommodated by GNDs, which produce back-stress strengthening at the yield point and back-stress work hardening during subsequent plastic deformation (Fig. 13b) [21, 26, 31]. Second, the interfaces between the soft lamellar coarse grains and hard nano-grain/nano-twin domains will also produce GNDs and long-range back stress although the strength is not as large as the first case.

Conclusions

By means of the conventional cold rolling, the heterogeneous lamella structure (HLS) was produced, which is characterized with lamellar coarse grains sandwiched between domains consisting of nano-grains and nano-twins in a 316L stainless steel. This original HLS produced high tensile strength (yield strength of ~ 1421 MPa) but a limited ductility (uniform elongation of ~ 1.6%). Subsequent annealing at 750 °C for 5–25 min led to the evolution of HLS, forming soft domains with recrystallized domains. A superior combination of high yield strength (~ 1 GPa) and an elongation-to-failure of ~ 20% was obtained for the sample annealed for 10 min. Back-stress strengthening and work hardening are believed to have played a significant role in producing the superior mechanical properties. The technique developed here is conducive to large-scale industrial production at low cost.

Acknowledgements

The authors acknowledge the financial support of National Key R&D Program of China (2017YFA0204403), National Natural Science Foundation of China (Grant Nos. 51301092 and 51741106 (Yusheng Li), No. 51601094 (Yang Cao)), the Jiangsu

Key Laboratory of Advanced Micro & Nano Materials and Technology, and the Pangu Foundation. Yuntian Zhu acknowledges the support of the US Army Research Office (W911 NF-17-1-0350). EBSD and TEM were performed in the Materials Characterization and Research Center of the Nanjing University of Science and Technology.

Compliance with ethical standards

Conflicts of interest The authors declare that they have no conflict of interest.

References

[1] Lo KH, Shek CH, Lai JKL (2009) Recent developments in stainless steels. Mater Sci Eng R 65:39–104

[2] Martienssen W, Warlimont H (2005) Springer handbook of condensed matter and materials data. Springer, Berlin

[3] Belyakov A, Kimura Y, Tsuzaki K (2006) Microstructure evolution in dual-phase stainless steel during severe deformation. Acta Mater 54:2521–2532

[4] Odnobokova M, Belyakov A, Kaibyshev R (2015) Effect of severe cold or warm deformation on microstructure evolution and tensile behavior of a 316L stainless steel. Adv Eng Mater 17:1812–1820

[5] Lu K, Lu J (2004) Nanostructured surface layer on metallic materials induced by SMAT. Mater Sci Eng A 375–377:38–45

[6] Chen XH, Lu J, Lu L, Lu K (2005) Tensile properties of a nanocrystalline 316L austenitic stainless steel. Scr Mater 52:1039–1044

[7] Valiev RZ, Islamgaliev RK, Alexandrov IV (2000) Bulk nanostructured materials from severe plastic deformation. Prog Mater Sci 45:103–189

[8] Ueno H, Kakihata K, Kaneko Y, Hashimoto S, Vinogradov A (2011) Nanostructurization assisted by twinning during equal channel angular pressing of metastable 316L stainless steel. J Mater Sci 46:4276–4283. https://doi.org/10.1007/s10853-011-5303-4

[9] Huang CX, Yang G, Gao YL, Wu SD, Zhang ZF (2008) Influence of processing temperature on the microstructures and tensile properties of 304L stainless steel by ECAP. Mater Sci Eng A 485:643–650

[10] Huang CX, Hu WP, Wang QY, Wang C, Yang G, Zhu YT (2015) An ideal ultrafine-grained structure for high strength and high ductility. Mater Res Lett 3:88–94

[11] Saito N, Mabuchi M, Nakanishi M, Shigematsu I, Yamauchi G, Nakamura M (2001) Application of equal channel angular extrusion on strengthening of ferritic stainless steel. J Mater Sci 36:3229–3232. https://doi.org/10.1023/A:1017990420563

[12] An XH, Lin QY, Wu SD, Zhang ZF, Figueiredo RB, Gao N, Langdon TG (2011) The influence of stacking fault energy on the mechanical properties of nanostructured Cu and Cu-Al alloys processed by high-pressure torsion. Scr Mater 64:954–957

[13] Gubicza J, El-Tahawy M, Huang Y, Choi H, Choe H, Labar JL, Langdon TG (2016) Microstructure, phase composition and hardness evolution in 316L stainless steel processed by high-pressure torsion. Mater Sci Eng A 657:215–223

[14] Ma E, Zhu T (2017) Towards strength-ductility synergy through the design of heterogeneous nanostructures in metals. Mater Today 20:323–331

[15] Zhu YT, Liao XZ (2004) Nanostructured metals: retaining ductility. Nat Mater 3:351–352

[16] Lu K (2016) Stabilizing nanostructures in metals using grain and twin boundary architectures. Nat Rev Mater 1:16019. https://doi.org/10.1038/natrevmats.2016.19

[17] Zhao YH, Bingert JF, Liao XZ, Cui BZ, Han K, Sergueeva AV, Mukherjee AK, Valiev RZ, Langdon TG, Zhu YT (2006) Simultaneously increasing the ductility and strength of ultra-fine-grained pure copper. Adv Mater 18:2949–2953

[18] Fang TH, Li WL, Tao NR, Lu K (2011) Revealing extraordinary intrinsic tensile plasticity in gradient nano-grained copper. Science 331:1587–1590

[19] Wu XL, Jiang P, Chen L, Yuan FP, Zhu YT (2014) Extraordinary strain hardening by gradient structure. Proc Natl Acad Sci USA 111:7197–7201

[20] Wu XL, Yang MX, Yuan FP, Chen L, Zhu YT (2016) Combining gradient structure and TRIP effect to produce austenite stainless steel with high strength and ductility. Acta Mater 112:337–346

[21] Yang MX, Pan Y, Yuan FP, Zhu YT, Wu XL (2016) Back stress strengthening and strain hardening in gradient structure. Mater Res Lett 4:145–151

[22] Wang Y, Chen M, Zhou F, Ma E (2002) High tensile ductility in a nanostructured metal. Nature 419:912–915

[23] Mahesh BV, Raman RKS, Koch CC (2012) Bimodal grain size distribution: an effective approach for improving the mechanical and corrosion properties of Fe-Cr-Ni alloys. J Mater Sci 47:7735–7743. https://doi.org/10.1007/s10853-012-6686-6

[24] Sekiguchi T, Ono K, Fujiwara H, Ameyama K (2010) New microstructure design for commercially pure titanium with outstanding mechanical properties by mechanical milling and hot roll sintering. Mater Trans 51:39–45

[25] Ma XL, Huang CX, Moering J, Ruppert M, Hoppel HW, Goken M, Narayan J, Zhu YT (2016) Mechanical properties

of copper/bronze laminates: role of interfaces. Acta Mater 116:43–52

[26] Wu XL, Yang MX, Yuan FP, Wu GL, Wei YJ, Huang XX, Zhu YT (2015) Heterogeneous lamella structure unites ultrafine-grain strength with coarse-grain ductility. Proc Natl Acad Sci USA 112:14501–14505

[27] Xing JX, Yuan FP, Wu XL (2017) Enhanced quasi-static and dynamic shear properties by heterogeneous gradient and lamella structures in 301 stainless steels. Mater Sci Eng A 680:305–316

[28] Yan FK, Liu GZ, Tao NR, Lu K (2012) Strength and ductility of 316L austenitic stainless steel strengthened by nano-scale twin bundles. Acta Mater 60:1059–1071

[29] Hirota N, Yin FX, Inoue T, Azuma T (2008) Recrystallization and grain growth behavior in severe cold-rolling deformed SUS316L steel under anisothermal annealing condition. ISIJ Int 48:475–482

[30] Belyakov A, Kipelova A, Odnobokova M, Shakhova I, Kaibyshev R (2014) Development of ultrafine grained austenitic stainless steels by large strain deformation and annealing. Mater Sci Forum 783–786:651–656

[31] Wu XL, Zhu YT (2017) Heterogeneous materials: a new class of materials with unprcedented mechanical properties. Mater Res Lett 5:527–532

[32] Tsakiris V, Edmonds DV (1999) Martensite and deformation twinning in austenitic steels. Mater Sci Eng A 273–275:430–436

[33] Eskandari M, Najafizadeh A, Kermanpur A (2009) Effect of strain-induced martensite on the formation of nanocrystalline 316L stainless steel after cold rolling and annnealing. Mater Sci Eng A 519:46–50

[34] Kumar BR, Das SK, Mahato B, Ghosh RN (2010) Role of strain-induced martensite on microstructural evolution during annealing of metastable austenitic stainless steel. J Mater Sci 45:911–918. https://doi.org/10.1007/s10853-009-4020-8

[35] Roland T, Retraint D, Lu K, Lu J (2007) Enhanced mechanical behavior of nanocrystallised stainless steel and its thermal stability. Mater Sci Eng A 445–446:281–288

[36] Huang HW, Wang ZB, Lu J, Lu K (2015) Fatigue behaviors of AISI 316L stainless steel with a gradient nanostructured surface layer. Acta Mater 87:150–160

[37] Meyers MA, Xu YB, Xue Q, Perez-Prado MT, McNelley TR (2003) Microstructural evolution in adiabatic shear localization in stainless steel. Acta Mater 51:1307–1325

[38] Li YS, Tao NR, Lu K (2008) Microstructural evolutionand nanostructure formation in copper during dynamic plastic deformation at cryogenic temperatures. Acta Mater 56:230–241

[39] Donadille C, Valle R, Dervin P, Penelle R (1989) Development of texture and microstructure during cold-rolling and annealing of FCC alloys: example of an austenitic stainless steel. Acta Metall 37:1547–1571

[40] Schino AD, Kenny JM, Abbruzzese G (2002) Analysis of the recrystallization and grain growth processes in AISI 316 stainless steel. J Mater Sci 37:5291–5298. https://doi.org/10.1023/A:1021068806598

[41] Liu XC, Zhang HW, Lu K (2013) Strain-induced ultrahard and ultrastable nanolaminated structure in nickel. Science 342:337–340

[42] Arshad MA, Maaroufi AK (2015) Relationship between Johnson-Mehl-Avrami and Sestak-Berggren models in the kinetics of crystallization in amorphous materials. J Non-crystall Solids 413:53–58

[43] Chowdhury SG, Das S, De PK (2005) Cold rolling behaviour and textural evolution in AISI 316L austenitic stainless steel. Acta Mater 53:3951–3959

[44] An XH, Lin QY, Sha G, Huang MX, Ringer SP, Zhu YT, Liao XZ (2016) Microstructural evolution and phase transformation in twinning-induced plasticity steel induced by high-pressure torsion. Acta Mater 109:300–313

[45] Kumar BR, Ghosh M (2007) Surface and mid-plane texture evolution in austenite phase of cold rolled austenitic stainless steels. Mater Sci Eng A 457:236–245

[46] Odnobokova M, Kipelova A, Belyakov A, Kaibyshev R (2014) Microstructure evolution in a 316L stainless steel subjected to multidirectional forging and unidirectional bar rolling. IOP Conf Series Mater Sci Eng 63:012060. https://doi.org/10.1088/1757-899X/63/1/012060

[47] Xue Q, Liao XZ, Zhu YT, Gray GT III (2005) Formation mechanisms of nanostructures in stainless steel during high-strain-rate severe plastic deformation. Mater Sci Eng A 410–411:252–256

[48] Miura H, Kobayashi M, Todaka Y, Watanable C, Aoyagi Y, Sugiura N, Yoshinaga N (2017) Heterogeneous nanostructure developed in heavily cold-rolled stainless steels and the specific mechanical properties. Scr Mater 133:33–36

[49] Xue Q, Cerreta EK, Gray GT III (2007) Microstructural characteristics of post-shear localization in cold-rolled 316L stainless steel. Acta Mater 55:691–704

[50] Hu J, Shi YN, Sauvage X, Sha G, Lu K (2017) Grain boundary stability governs hardening and softening in extremely fine nanograined metals. Science 355:1292–1296

[51] Yanushkevich Z, Lugovskaya A, Belyakov A, Kaibyshev R (2016) Deformation microstructures and tensile properties of an austenitic stainless steel subjected to multiple warm rolling. Mater Sci Eng A 667:279–285

[52] Ucok I, Ando T, Grant NJ (1991) Property enhancement in type 316L stainless steel by spray forming. Mater Sci Eng A 133:284–287

[53] Wu XL, Jiang P, Chen L, Zhang JF, Yuan FP, Zhu YT (2014) Synergetic strengthening by gradient structure. Mater Res Lett 2:185–191

[54] You ZS, Li XY, Gui LJ, Lu QH, Zhu T, Gao HJ, Lu L (2013) Plastic anisotropy and associated deformation mechanisms in nanotwinned metals. Acta Mater 61:217–227

[55] Zhu T, Gao HJ (2012) Plastic deformation mechanism in nanotwinned metals: an insight from molecular dynamics and mechanistic modeling. Scr Mater 66:843–848

[56] Zhu YT, Liao XZ, Wu XL (2012) Deformation twinning in nanocrystalline materials. Prog Mater Sci 57:1–62

[57] Eskandari M, Zarei-Hanzaki A, Abedi HR (2013) An investigation into the room temperature mechanical properties of nanocrystalline austenitic stainless steels. Mater Des 45:674–681

[58] Valiev RZ, Estrin Y, Horita Z, Langdon TG, Zehetbauer MJ, Zhu YT (2016) Fundamentals of superior properties in bulk nanoSPD materials. Mater Res Lett 4:1–21